The Astrophysical Journal, 834:209 (5pp), 2017 January 10 doi:10.3847/1538-4357/834/2/209

PROPELLER EFFECT IN THE TRANSIENT X-RAY PULSAR SMC X-2

Alexander A. Lutovinov[1,2], Sergey S. Tsygankov[3], Roman A. Krivonos[1], Sergey V. Molkov[1], and Juri Poutanen[3,4]
[1] Space Research Institute, Russian Academy of Sciences, Profsoyuznaya 84/32, 117997 Moscow, Russia
[2] Moscow Institute of Physics and Technology, Moscow region, Dolgoprudnyi, Russia
[3] Tuorla Observatory, Department of Physics and Astronomy, University of Turku, Väisäläntie 20, FI-21500 Piikkiö, Finland
[4] Nordita, KTH Royal Institute of Technology and Stockholm University, Roslagstullsbacken 23, SE-10691 Stockholm, Sweden
Received 2016 July 13; revised 2016 October 15; accepted 2016 October 28; published 2017 January 13

ABSTRACT

We report the results of the monitoring campaign of the transient X-ray pulsar SMC X-2 performed with the *Swift*/XRT telescope over the period of 2015 September–2016 January during the Type II outburst. During this event, the bolometric luminosity of the source ranged from $\simeq 10^{39}$ down to several $\times 10^{34}$ erg s^{-1}. Moreover, we discovered its dramatic drop by a factor of more than 100 below the limiting value of $L_{\rm lim} \simeq 4 \times 10^{36}$ erg s^{-1}, which can be interpreted as a transition to the propeller regime. These measurements make SMC X-2 the sixth pulsating X-ray source where such a transition is observed and allow us to estimate the magnetic field of the neutron star in the system $B \simeq 3 \times 10^{12}$ G, which is in agreement with independent results of the spectral analysis.

Key words: accretion, accretion disks – magnetic fields – stars: individual (SMC X-2) – X-rays: binaries

1. INTRODUCTION

The Small Magellanic Cloud (SMC) is a Milky Way satellite situated at the distance of $d \simeq 62$ kpc (Haschke et al. 2012). This galaxy is extremely rich in Be X-ray binary systems, harboring a neutron star orbiting around an OBe companion (see a recent review by Coe & Kirk 2015, and references therein). SMC X-2 was discovered at an early stage of SMC study (Clark et al. 1978) during the Type II outburst, with an X-ray luminosity in the 2–11 keV energy band of about 10^{38} erg s^{-1}. The pulsating nature of the source was established during the second registered outburst, when pulsations with a period of $P_{\rm spin} \simeq 2.37$ s were detected by the *RXTE* observatory from the sky region around SMC X-2 (Corbet et al. 2001) and were later confirmed using the *ASCA* data (Yokogawa et al. 2001). The pulsar magnetic field was not known until now, but some data hint at the cyclotron line detection in the SMC X-2 spectrum near ∼27 keV, which was recently reported by Jaisawal & Naik (2016).

The optical counterpart of SMC X-2 was not unambiguously identified for quite a long time because two different stars of an early spectral type are located near the X-ray position of the source with the angular separation of only 2.″5. Only recent monitoring observations by the OGLE experiment revealed a variability of one of these stars with a period of $P_{\rm orb} = 18.62 \pm 0.02$ days (Schurch et al. 2011), which is in agreement with periodical variations of the pulse period detected by the *RXTE* and *Swift* observatories at $P_{\rm orb} \simeq 18.4$ days (Townsend et al. 2011; La Palombara et al. 2016). This periodicity was interpreted as an orbital period in the system that, in combination with the pulse period of $P_{\rm spin} \simeq 2.37$ s, places SMC X-2 in the Be-system region in the Corbet diagram (Corbet 1986).

The transient nature of a majority of Be systems is ideally suited for studying the magnetic field, for investigating luminosity-dependent accretion processes and the geometry of the system, as well as for learning about the interaction of the accreted matter with the neutron star magnetosphere (see Negueruela 1998; Reig 2011; Poutanen et al. 2013; Walter et al. 2015 for reviews and current physical models). One of the most interesting and straightforward manifestations of such an interaction is the transition of the accreting neutron star to the so-called propeller regime. The physical aspects of this regime were considered by Illarionov & Sunyaev (1975), who showed that under some conditions the accreted matter can be stopped by the centrifugal barrier set-up by the rapidly rotating magnetosphere of the strongly magnetized neutron star. This should lead to a dramatic drop of the X-ray intensity of the source. The moment of transition from the normal accretion regime to the propeller one depends on a combination of three physical parameters of the system—the pulse period, the magnetic moment (or magnetic field strength) of the neutron star, and the accretion rate. Because the pulse period and the accretion rate can be derived from observations, the detection of the propeller effect provides us with an independent estimation of the neutron star magnetic field. This knowledge is very important, as the magnetic field is one of the fundamental parameters governing observed properties of neutron stars.

Until recently, only a few cases of possible transitions into the propeller regime in accreting millisecond and X-ray pulsars were reported (Stella et al. 1986; Cui 1997; Campana et al. 2001, 2008). Recently, the propeller effect was also discovered in the first pulsating ultra-luminous X-ray source M82 X-2 (Tsygankov et al. 2016b). This discovery initiated a special monitoring program of transient X-ray pulsars with the *Swift*/XRT telescope, which searches for the propeller effect in other sources. First results of this program were published by Tsygankov et al. (2016a) for two well-known transient X-ray pulsars, V 0332+53 and 4U 0115+634, where the propeller effect was firmly established.

In this paper, we report a discovery of the propeller effect and the consequent determination of the magnetic field strength in another transient X-ray pulsar SMC X-2.

2. DATA ANALYSIS

SMC X-2 entered into a new outburst at the end of 2015 September and immediately started to be monitored with the *Swift*/XRT telescope (Kennea et al. 2015). The observations (totaling around 150 individual pointings) were performed from 2015 September 24 to 2016 January 25 in the Windowed

Timing (WT) and Photon Counting (PC) modes, depending on the source brightness. Final products (the spectrum in each observation) were prepared using online tools provided by the UK Swift Science Data Centre (Evans et al. 2009).[5] The spectra were grouped to have at least 1 count per bin and were fitted in the XSPEC package using the Cash statistic (Cash 1979). To avoid any problems caused by the calibration uncertainties at low energies,[6] we restricted our spectral analysis to the 0.7–10 keV band.

The obtained spectra in the source's high state can be well-fitted with a simple power-law model, which was modified by the interstellar absorption at low energies in the form of the PHABS model in the XSPEC package. We found that the hydrogen column density agrees well with the interstellar one in this direction. Therefore, in the following analysis, it was fixed at $N_{\rm H} = 3.4 \times 10^{21}$ cm^{-2} (Kalberla et al. 2005). To calculate the unabsorbed source flux, the CFLUX routine from the XSPEC package was used. In the low state, the source was not detected in any single observation. Therefore we averaged them into two groups, according to the observational dates. The first group includes observations performed during the second half of 2015 December (three observations), just after the expected transition to the propeller regime. The second group includes observations performed in 2016 January (11 observations). Again, the source was not detected in either group, and only upper limits to its flux were obtained based on the XRT sensitivity curve (Burrows et al. 2005). The log of *Swift*/XRT observations, including the time of observations, exposure, mode, and unabsorbed flux (or upper limits), is presented in Table 1.

SMC X-2 has been observed several times with the *NuSTAR* observatory, which allowed us to reconstruct its broadband spectrum in the 3–79 keV energy band for different luminosity levels and allowed us to obtain the bolometric correction of the flux observed by XRT in the 0.5–10 keV energy band to the flux in the 0.5–100 keV energy band that can be considered as bolometric. The analysis of the broadband spectrum of SMC X-2 was presented by Jaisawal & Naik (2016), therefore we will not discuss it in detail. Here we only would like to mention that it can be well described by the CUTOFF model, with the inclusion of the thermal blackbody component with the temperature of $\simeq$1 keV and the cyclotron absorption line at the energies of 28–30 keV. Note that the latter demonstrates a negative correlation with the source luminosity (see also Jaisawal & Naik 2016), similar to that observed in several other bright X-ray transient pulsars—4U 0115+63 (Nakajima et al. 2006; Tsygankov et al. 2007) and V 0332+53 (Tsygankov et al. 2010). The ratio of fluxes in the 0.5–100 and 0.5–10 keV energy bands also depends on the luminosity and lies in the range 2.2–2.8. Thus, for the following estimations, we used the averaged value of 2.5. All luminosities discussed below were corrected for the absorption as well.

The bolometric luminosity of SMC X-2, corrected for the absorption, is presented in Figure 1. There are (at least) three interesting features in this light curve.

1. The maximum luminosity is about 10^{39} erg s^{-1}, which exceeds the standard Eddington limit for the neutron star by a factor of five. This implies that at such a high accretion rate, the accretion column should be formed at

[5] http://www.swift.ac.uk/user_objects/
[6] http://www.swift.ac.uk/analysis/xrt/digest_cal.php

Table 1
Swift/XRT Observations of the Source SMC X-2

Obs Id	Date MJD	Exposure (s)	Flux[a] (10^{-10} erg s^{-1} cm^{-2})	Mode
00034073001	57289.6471	1979	$4.52^{+0.22}_{-0.21}$	WT
00034073002	57290.9811	1656	$5.08^{+0.71}_{-0.64}$	WT
00034073003	57292.9435	1580	$6.28^{+0.09}_{-0.09}$	WT
00034073005	57294.5720	1799	$6.28^{+0.12}_{-0.11}$	WT
00034073007	57296.3051	1947	$6.31^{+0.13}_{-0.12}$	WT
00034073008	57297.1372	1888	$5.53^{+0.08}_{-0.08}$	WT
00034073009	57298.6319	1908	$5.09^{+0.07}_{-0.06}$	WT
00034073010	57299.7248	1760	$4.91^{+0.10}_{-0.09}$	WT
00034073011	57300.8618	491	$4.27^{+0.13}_{-0.14}$	WT
00034073012	57299.7119	405	$4.76^{+0.18}_{-0.17}$	WT
00034073013	57301.5726	224	$3.15^{+0.19}_{-0.18}$	WT
00034073014	57301.5834	1597	$2.81^{+0.07}_{-0.08}$	WT
00034073015	57302.8351	294	$3.24^{+0.15}_{-0.15}$	WT
00034073016	57302.8475	1758	$3.78^{+0.10}_{-0.10}$	WT
00034073017	57303.3978	183	$2.67^{+0.22}_{-0.20}$	WT
00034073018	57303.4044	1965	$3.70^{+0.09}_{-0.08}$	WT
00034073019	57304.8662	301	$3.17^{+0.15}_{-0.15}$	WT
00034073020	57304.8727	1979	$3.30^{+0.06}_{-0.05}$	WT
00034073021	57305.8641	388	$2.79^{+0.12}_{-0.11}$	WT
00034073022	57305.8710	1984	$3.25^{+0.05}_{-0.06}$	WT
00034073023	57306.7901	361	$2.72^{+0.13}_{-0.12}$	WT
00034073024	57306.7974	1991	$2.94^{+0.05}_{-0.05}$	WT
00081771001	57307.9317	471	$2.28^{+0.10}_{-0.10}$	WT
00081771002	57307.9366	1497	$2.83^{+0.06}_{-0.06}$	WT
00034073025	57308.7849	410	$2.17^{+0.11}_{-0.11}$	WT
00034073026	57308.7924	2158	$2.54^{+0.05}_{-0.05}$	WT
00034073027	57309.3130	288	$2.83^{+0.15}_{-0.15}$	WT
00034073028	57309.3141	1005	$2.59^{+0.07}_{-0.07}$	WT
00034073029	57310.5200	348	$2.17^{+0.11}_{-0.10}$	WT
00034073030	57310.5274	2088	$2.48^{+0.05}_{-0.05}$	WT
00034073031	57311.6110	381	$2.23^{+0.11}_{-0.11}$	WT
00034073032	57311.6184	4008	$2.34^{+0.04}_{-0.03}$	WT
00034073033	57312.4362	1358	$2.07^{+0.05}_{-0.05}$	WT
00034073034	57312.4409	4500	$2.01^{+0.03}_{-0.03}$	WT
00034073035	57313.4667	520	$1.87^{+0.08}_{-0.08}$	WT
00034073037	57314.8068	224	$1.87^{+0.14}_{-0.13}$	WT
00034073038	57314.7121	1560	$1.77^{+0.05}_{-0.04}$	WT
00034073039	57315.2938	524	$1.74^{+0.09}_{-0.08}$	WT
00034073040	57315.3039	4355	$1.55^{+0.03}_{-0.02}$	WT
00034073041	57316.6603	521	$1.68^{+0.08}_{-0.08}$	WT
00034073042	57316.6686	3953	$1.74^{+0.03}_{-0.03}$	WT
00034073043	57317.2878	943	$1.56^{+0.06}_{-0.06}$	WT
00034073044	57317.2969	8329	$1.42^{+0.02}_{-0.02}$	WT
00034073045	57318.3171	605	$1.48^{+0.09}_{-0.08}$	WT
00034073047	57319.4473	151	$1.16^{+0.21}_{-0.18}$	WT
00034073048	57319.4910	2228	$1.25^{+0.04}_{-0.04}$	WT
00034073049	57320.4445	391	$1.21^{+0.10}_{-0.09}$	WT
00034073051	57321.3082	496	$1.35^{+0.08}_{-0.08}$	WT
00034073052	57321.3155	3938	$1.24^{+0.03}_{-0.03}$	WT
00034073054	57322.3206	744	$1.19^{+0.06}_{-0.06}$	WT
00034073055	57323.1040	600	$1.12^{+0.07}_{-0.06}$	WT
00034073056	57323.1123	3484	$1.03^{+0.03}_{-0.03}$	WT
00034073058	57324.6376	312	$1.30^{+0.16}_{-0.14}$	PC
00034073059	57325.1331	720	$1.08^{+0.07}_{-0.06}$	WT
00034073060	57325.1382	3678	$1.15^{+0.03}_{-0.03}$	WT
00034073061	57326.3635	778	$1.01^{+0.06}_{-0.06}$	WT
00034073062	57326.3673	3905	$1.07^{+0.03}_{-0.03}$	WT

Table 1
(Continued)

Obs Id	Date MJD	Exposure (s)	Flux[a] (10^{-10} erg s^{-1} cm^{-2})	Mode
00034073063	57327.1952	744	$0.93^{+0.07}_{-0.04}$	WT
00034073064	57327.1999	2325	$1.07^{+0.04}_{-0.04}$	WT
00034073065	57328.1589	549	$0.93^{+0.07}_{-0.06}$	WT
00034073067	57337.9300	448	$0.71^{+0.07}_{-0.05}$	WT
00034073068	57337.9357	1389	$0.91^{+0.04}_{-0.06}$	WT
00034073070	57338.7359	1703	$0.91^{+0.04}_{-0.02}$	WT
00034073071	57339.7532	550	$0.66^{+0.06}_{-0.04}$	WT
00034073072	57339.7619	2365	$0.85^{+0.04}_{-0.02}$	WT
00034073073	57340.8150	134	$0.66^{+0.13}_{-0.11}$	WT
00034073074	57340.7626	1750	$0.76^{+0.04}_{-0.03}$	WT
00034073075	57341.6784	360	$0.60^{+0.07}_{-0.05}$	WT
00034073076	57341.7213	2016	$0.63^{+0.03}_{-0.03}$	WT
00034073077	57342.8066	294	$0.78^{+0.09}_{-0.07}$	WT
00034073078	57342.8219	1038	$0.79^{+0.04}_{-0.05}$	WT
00034073079	57343.6030	736	$0.63^{+0.06}_{-0.04}$	WT
00034073080	57343.6094	1777	$0.74^{+0.03}_{-0.05}$	WT
00034073081	57345.9011	178	$0.41^{+0.12}_{-0.10}$	WT
00034073082	57345.9076	1995	$0.63^{+0.03}_{-0.03}$	WT
00034073083	57346.3602	384	$0.56^{+0.07}_{-0.05}$	WT
00034073084	57346.3676	1989	$0.51^{+0.04}_{-0.03}$	WT
00034073085	57347.6270	236	$0.58^{+0.10}_{-0.09}$	WT
00034073086	57347.6336	1922	$0.52^{+0.02}_{-0.04}$	WT
00034073087	57348.5565	170	$0.49^{+0.09}_{-0.08}$	WT
00034073088	57348.5630	1985	$0.51^{+0.02}_{-0.02}$	WT
00034073089	57349.3533	277	$0.49^{+0.06}_{-0.06}$	WT
00034073090	57349.3554	1171	$0.58^{+0.04}_{-0.04}$	WT
00034073091	57350.4840	252	$0.48^{+0.07}_{-0.06}$	WT
00034073092	57350.4907	1703	$0.52^{+0.04}_{-0.02}$	WT
00034073093	57351.5410	240	$0.50^{+0.09}_{-0.08}$	WT
00034073094	57351.5479	2338	$0.58^{+0.03}_{-0.04}$	WT
00034073095	57352.7369	290	$0.38^{+0.05}_{-0.05}$	WT
00034073096	57352.7434	2046	$0.45^{+0.03}_{-0.02}$	WT
00034073099	57354.5984	323	$0.35^{+0.05}_{-0.05}$	WT
00034073100	57354.6058	2232	$0.42^{+0.02}_{-0.02}$	WT
00034073102	57355.7453	2101	$0.46^{+0.03}_{-0.03}$	WT
00034073103	57356.5266	444	$0.26^{+0.05}_{-0.04}$	WT
00034073104	57356.5342	1972	$0.45^{+0.03}_{-0.03}$	WT
00034073105	57357.1884	242	$0.30^{+0.04}_{-0.04}$	WT
00034073106	57357.1953	2165	$0.41^{+0.02}_{-0.03}$	WT
00034073108	57358.3574	977	$0.35^{+0.03}_{-0.03}$	WT
00034073109	57359.1477	273	$0.22^{+0.05}_{-0.04}$	WT
00034073110	57359.1553	1988	$0.27^{+0.02}_{-0.02}$	WT
00034073111	57360.2485	391	$0.22^{+0.05}_{-0.04}$	WT
00034073112	57360.2559	1981	$0.25^{+0.02}_{-0.02}$	WT
00034073113	57361.3750	3266	$0.23^{+0.05}_{-0.04}$	WT
00034073114	57361.3819	1983	$0.22^{+0.02}_{-0.02}$	WT
00034073116	57362.1417	1297	$0.15^{+0.02}_{-0.02}$	WT
00034073117	57363.1686	348	$0.13^{+0.05}_{-0.04}$	WT
00034073118	57363.1778	2104.6	$0.13^{+0.02}_{-0.02}$	WT
00034073119	57364.3003	147.5	$0.17^{+0.09}_{-0.06}$	WT
00034073120	57364.3073	1987.7	$0.09^{+0.01}_{-0.01}$	WT
00034073121	57365.3633	218.3	$0.08^{+0.05}_{-0.03}$	WT
00034073122	57365.3701	1977.6	$0.11^{+0.02}_{-0.02}$	WT
00034073123	57366.1267	175.0	$0.07^{+0.08}_{-0.04}$	WT
00034073124	57366.0685	1111.0	$0.08^{+0.02}_{-0.01}$	WT
00034073127	57368.4540	114.3	$0.08^{+0.06}_{-0.04}$	WT
00034073128	57368.4602	861.8	$0.07^{+0.02}_{-0.01}$	WT
00034073129	57369.1544	368.2	$0.10^{+0.04}_{-0.03}$	WT
00034073130	57369.1618	1340.8	$0.04^{+0.01}_{-0.01}$	WT
00034073131	57370.9811	95.7	$0.07^{+0.09}_{-0.04}$	WT
00034073132	57370.9893	1231.4	$0.03^{+0.01}_{-0.01}$	WT
00034073133	57371.2809	221.6	$0.29^{+0.13}_{-0.14}$	WT
00034073134	57371.2871	1782.7	$0.06^{+0.02}_{-0.01}$	WT
		Group 1		
00034073135	57375.5719	1938	0.0003[b]	PC
00034073136	57376.6368	1583	…	PC
00034073137	57378.2005	1568	…	PC
		Group 2		
00034073139	57392.3539	737	0.00016[b]	PC
00034073140	57394.9368	1653	…	PC
00034073141	57396.2917	912	…	PC
00034073142	57398.4597	1586	…	PC
00034073143	57400.5460	1900	…	PC
00034073144	57402.3410	1836	…	PC
00034073145	57404.6973	2379	…	PC
00034073146	57406.3691	1226	…	PC
00034073147	57408.3840	1671	…	PC
00034073148	57410.7484	1848	…	PC
00034073149	57412.7004	812	…	PC

Notes.
[a] Unabsorbed flux in the 0.5–10 keV energy range.
[b] Upper limit in the 0.5–10 keV energy range.

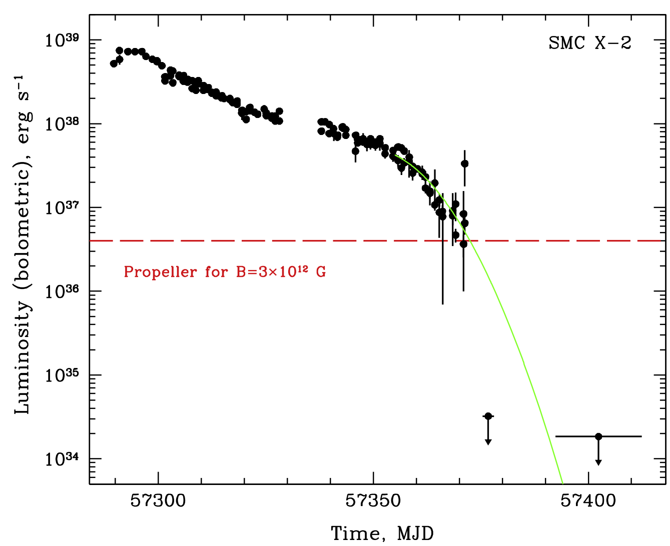

Figure 1. Evolution of the bolometric luminosity of SMC X-2 during the 2015–2016 outburst. Luminosity is calculated from the unabsorbed flux derived from *Swift*/XRT data under the assumption of the distance $d = 62$ kpc and a bolometric correction factor of 2.5 (see Section 2). Two upper limits were obtained by averaging 3 and 11 observations, respectively, with very low count statistics (note that all of them were performed in the PC mode). The solid green line illustrates the flux decay law right before the transition to the propeller regime and was obtained by fitting the light curve with a Gaussian function (see, e.g., Campana et al. 2014). The horizontal dashed line shows the approximate limiting luminosity when the propeller regime sets in.

the neutron star surface, and the magnetic field on the neutron star's surface should be at least $\sim 10^{12}$ G (Mushtukov et al. 2015).

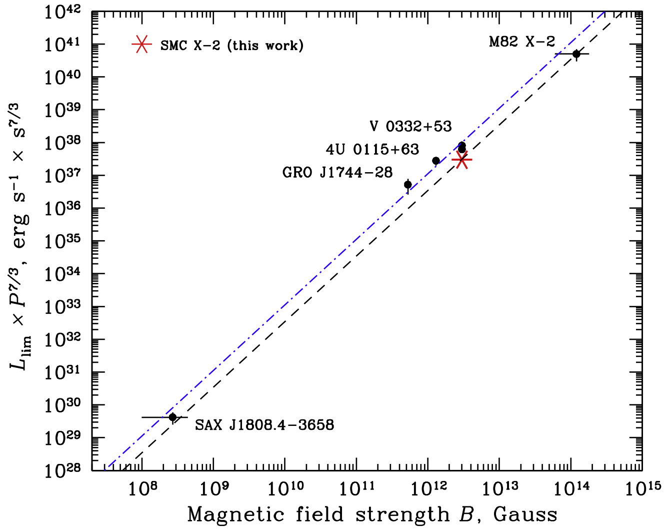

Figure 2. Observed correlation between a combination of the propeller limiting luminosity and the pulse period, $L_{\rm lim}P^{7/3}$, and the magnetic field strength B at the neutron star surface (independent measurements) for five sources (for details, see Tsygankov et al. 2016a). The dashed and dotted–dashed lines represent the theoretical dependence from Equation (1) assuming standard parameters for a neutron star ($M = 1.4M_\odot$, $R = 10$ km), and $k = 0.5$ and $k = 0.7$, respectively. The red star indicates the position of SMC X-2 for the case of $k = 0.5$ and the limiting luminosity $L_{\rm lim} \simeq 4 \times 10^{36}$ erg s^{-1}.

2. The decay of the light curve is nearly exponential during the first two months of the outburst (excluding the last dozen days).
3. There is a dramatic drop (by a factor of more than 100) of the source luminosity on MJD 57370 at around $L_{\rm lim} \simeq (4 \pm 1) \times 10^{36}$ erg s^{-1} (see the red dashed line). Note that there is a time gap (about four days) between the last observation when the source was significantly detected and the next one when the source was not detected already (see Table 1). Therefore, we take the limiting luminosity as the average luminosity between the last significant measurement and an extrapolation of our fit (see Gaussian in Figure 1) to the time of the next observation where the source was not detected. The uncertainty corresponds to the difference between that luminosity and the measured or extrapolated luminosities. This drastic change of the source luminosity is most likely related to its transition to the propeller regime.

Below we briefly discuss this effect and estimate physical parameters of the system SMC X-2, in particular the magnetic field strength of the neutron star.

3. ESTIMATE OF THE MAGNETIC FIELD

The main idea behind the propeller effect is that the accretion of matter onto a strongly magnetized neutron star is only possible if the velocity of the magnetic field lines is lower than the local Keplerian velocity at the magnetospheric radius ($R_{\rm m}$). This condition is only fulfilled in the case where the magnetospheric radius is smaller than the co-rotation radius ($R_{\rm c}$). Because of the dependence of the magnetospheric radius on the mass accretion rate and magnetic field strength, one can link the latter to the limiting luminosity, which corresponds to the onset of the propeller regime by equating the co-rotation and magnetospheric radii (Campana et al. 2002)

$$L_{\rm lim}(R) \simeq \frac{GM\dot{M}_{\rm lim}}{R} \simeq 4 \times 10^{37} k^{7/2} B_{12}^{2} P^{-7/3} M_{1.4}^{-2/3} R_{6}^{5} \text{ erg s}^{-1}, \quad (1)$$

where R_6 is the neutron star radius in units of 10^6 cm, $M_{1.4}$ is the neutron star mass in units of 1.4 $M_\odot$, P is the pulsar's rotational period in seconds, and B_{12} is the magnetic field strength in units of 10^{12} G on the neutron star surface under an assumption of the dipole configuration of the magnetic field. The factor k relates the magnetospheric radius in the case of disk accretion to the Alfvén radius calculated for spherical accretion ($R_{\rm m} = k \times R_{\rm A}$) and is usually assumed to be $k = 0.5$ (Ghosh & Lamb 1978).

Following from Equation (1), a detection of the transition of the pulsar to the propeller regime and the measurement of the corresponding limiting luminosity $L_{\rm lim}$ can be used to estimate the neutron star magnetic field. The validity of such an approach was recently proven by Tsygankov et al. (2016a), who compared several X-ray pulsars' magnetic field strengths obtained with this method to independently-determined values in an extremely wide range of magnetic fields, from 10^8 to 10^{14} G (see Figure 2).

For the standard parameters of a neutron star where $M = 1.4M_\odot$, $R = 10$ km, and $k = 0.5$, the measured limiting luminosity of $L_{\rm lim} \simeq 4 \times 10^{36}$ erg s^{-1} corresponds to the magnetic field strength $B = (3.0 \pm 0.4) \times 10^{12}$ G. Based on these estimations, we can predict that the cyclotron line should be observed in SMC X-2 at around 25 keV. This is in agreement with the independent measurement by the *NuSTAR* observatory (see above and Jaisawal & Naik 2016).

4. CONCLUSION

In this paper we have reported the discovery of the propeller effect in the bright transient X-ray pulsar SMC X-2. The dramatic drop of the source luminosity (by a factor of more than 100) on the timescale of a few days was revealed thanks to the monitoring campaign with the *Swift*/XRT telescope, which was organized during the Type II outburst registered from the source from 2015 September–2016 January. The luminosity drop occurred near the luminosity of $L_{\rm lim} \simeq 4 \times 10^{36}$ erg s^{-1}. Based on this measurement, we estimated the magnetic field strength of the neutron star in the SMC X-2 binary system as $B \simeq 3 \times 10^{12}$ G, which is typical for X-ray pulsars (see, e.g., a recent review by Walter et al. 2015) and confirmed independently by the results of the spectral analysis. Thus our discovery makes SMC X-2 the sixth known pulsating X-ray source where the propeller effect was observed.

This research has made use of *Swift*/XRT data provided by the UK Swift Science Data Centre at the University of Leicester. A.A.L., S.S.T., and S.V.M. acknowledge support from the Russian Science Foundation (grant 14-12-01287). J.P. thanks the Foundations' Professor Pool, the Finnish Cultural Foundation, and the Academy of Finland (grant 268740) for their financial support. The authors thank the anonymous referee for their useful comments.

REFERENCES

Burrows, D. N., Hill, J. E., Nousek, J. A., et al. 2005, SSRv, 120, 165
Campana, S., Brivio, F., Degenaar, N., et al. 2014, MNRAS, 441, 1984

Campana, S., Gastaldello, F., Stella, L., et al. 2001, ApJ, 561, 924
Campana, S., Stella, L., Israel, G. L., et al. 2002, ApJ, 580, 389
Campana, S., Stella, L., & Kennea, J. A. 2008, ApJL, 684, L99
Cash, W. 1979, ApJ, 228, 939
Clark, G., Doxsey, R., Li, F., Jernigan, J. G., & van Paradijs, J. 1978, ApJL, 221, L37
Coe, M. J., & Kirk, J. 2015, MNRAS, 452, 969
Corbet, R. H. D. 1986, MNRAS, 220, 1047
Corbet, R. H. D., Marshall, F. E., Coe, M. J., Laycock, S., & Handler, G. 2001, ApJL, 548, L41
Cui, W. 1997, ApJL, 482, L163
Evans, P. A., Beardmore, A. P., Page, K. L., et al. 2009, MNRAS, 397, 1177
Ghosh, P., & Lamb, F. K. 1978, ApJL, 223, L83
Haschke, R., Grebel, E. K., & Duffau, S. 2012, AJ, 144, 107
Illarionov, A. F., & Sunyaev, R. A. 1975, A&A, 39, 185
Jaisawal, G., & Naik, S. 2016, MNRAS, 461, L97
Kalberla, P., Burton, W., Hartmann, D., et al. 2005, A&A, 440, 775
Kennea, J. A., Burrows, D. N., Coe, M. J., et al. 2015, ATel, 8091, 1
La Palombara, N., Sidoli, L., Pintore, F., et al. 2016, MNRAS, 458, L74
Mushtukov, A. A., Suleimanov, V. F., Tsygankov, S. S., & Poutanen, J. 2015, MNRAS, 454, 2539
Nakajima, M., Mihara, T., Makishima, K., & Niko, H. 2006, ApJ, 646, 1125
Negueruela, I. 1998, A&A, 338, 505
Poutanen, J., Mushtukov, A. A., Suleimanov, V. F., et al. 2013, ApJ, 777, 115
Reig, P. 2011, Ap&SS, 332, 1
Schurch, M. P. E., Coe, M. J., McBride, V. A., et al. 2011, MNRAS, 412, 391
Stella, L., White, N. E., & Rosner, R. 1986, ApJ, 308, 669
Townsend, L. J., Coe, M. J., Corbet, R. H. D., & Hill, A. B. 2011, MNRAS, 416, 1556
Tsygankov, S. S., Lutovinov, A. A., Churazov, E. M., & Sunyaev, R. A. 2007, AstL, 33, 368
Tsygankov, S. S., Lutovinov, A. A., Doroshenko, V., et al. 2016a, A&A, 593, A16
Tsygankov, S. S., Lutovinov, A. A., & Serber, A. V. 2010, MNRAS, 401, 1628
Tsygankov, S. S., Mushtukov, A. A., Suleimanov, V. F., & Poutanen, J. 2016b, MNRAS, 457, 1101
Walter, R., Lutovinov, A. A., Bozzo, E., & Tsygankov, S. S. 2015, ARA&A, 23, 2
Yokogawa, J., Torii, K., Kohmura, T., & Koyama, K. 2001, PASJ, 53, 227